THE ASTROPHYSICAL JOURNAL, 296:461–468, 1985 September 15

RADIO AND X-RAY OBSERVATIONS OF G11.2−0.3 AND G41.1−0.3

R. H. BECKER
Physics Department, University of California at Davis
AND
T. MARKERT AND M. DONAHUE
Center for Space Research, MIT
Received 1985 February 14; accepted 1985 March 19

ABSTRACT

The supernova remnants G11.2−0.3 and G41.1−0.3 have been observed in radio and X-ray utilizing the VLA and *Einstein Observatory*, respectively. The acquired images reveal that both sources have shell morphologies and do not exhibit any clear indication of a central stellar remnant. In addition, both objects are relatively bright X-ray sources.

Subject headings: nebulae: supernova remnants — radio sources: identifications — X-rays: sources

I. INTRODUCTION

This paper is the sixth in a series which present high-resolution radio and X-ray images of small-diameter galactic supernova remnants (SNRs) (Becker and Szymkowiak 1981; Becker, Helfand, and Szymkowiak 1983: Andrews *et al.* 1983; Pye *et al.* 1984; Kriss *et al.* 1984). The rationale for this project is to provide a more complete sample of morphological traits of galactic SNRs. There are ~ 150 known galactic SNRs which have all been identified on the basis of their nonthermal radio emission coupled with their proximity to the galactic plane. When we think of SNRs, most of us conjure up a mental image of Cas A or the Crab Nebula, which serve as prototypes for shell and Crab-like remnants, respectively. The differences between these two forms can be explained in terms of the sources of energy driving the two remnants. The energy for Cas A is stored in the kinetic energy of the expanding shell of ejecta and is released at the remnant's extremity, while the energy for the Crab Nebula is stored in the rotational kinetic energy of the central neutron star and is released at the remnant's center.

Presumably, these two types of SNRs evolve from different types of progenitor stars, and it is interesting to speculate on what they are. To this end, it is desirable to determine all that we can about the spatial distribution and frequency of the different types of remnants. As a first step in this direction, it is necessary to observe and classify those galactic SNRs already cataloged. In fact, a significant fraction ($\sim 40\%$) of these objects are so poorly observed that classification is not presently possible. This is particularly true in light of the growing number of remnants which have attributes of both shell and Crab-like sources, such as G29.7−0.3 and G326.2−1.7 (Becker, Helfand, and Szymkowiak 1983; Caswell *et al.* 1975). These combination remnants can only be identified with images of comparable angular resolution at several wavelengths. This necessity has led us into a program of mapping galactic remnants at two radio wavelengths (6 and 20 cm) with the VLA[1] in a "scaled-array" configuration; i.e., the baselines utilized are scaled to the wavelength of the observation.

Where possible, these observations are supplemented by X-ray observations which also have the ability to discriminate between various remnant morphologies. In general, the X-ray emission from shell and Crab-like SNRs arise from thermal and nonthermal mechanisms, respectively, so that X-ray spectra can be used to distinguish the two morphologies. In addition, X-ray images have proved a powerful tool in discovering compact sources within SNRs (Helfand and Becker 1984).

In this paper we present radio and X-ray observations of two galactic SNRs, G11.2−0.3 and G41.1−0.3, sources for which high-resolution images have been previously unavailable.

II. G11.2−0.3

The radio source G11.2−0.3 has traditionally been considered a SNR and is included in catalogs by Downes (1971), Ilovaisky and Lequeux (1972), Green (1974), and Milne (1979). The radio flux from G11.2−0.3 has been reported from 80 MHz through 10.6 GHz, from which a spectral index of −0.55 can be estimated. Early radio images of G11.2−0.3 can be found in Shaver and Weiler (1976). Both these images were based on interferometric data with highly asymmetric UV coverage resulting in extremely elliptical beam patterns. Both works concluded that the data were consistent with a shell structure 4′ diameter. More recently, Downes (1984) published a 20 cm image comparable to that presented here.

Distance estimates for G11.2−0.3 are available from two sources. Radhakrishnan *et al.* (1972) obtained 21 cm absorption profiles for this source from which he inferred a lower limit for the distance of 4.5 kpc. Using the Σ–D relationship for SNRs, Milne (1979) inferred a distance of 11.9 kpc.

The remnant G11.2−0.3 is unusual insofar as it is one of only eight galactic remnants with which a historical supernova may be associated. Clark and Stephenson (1977) have suggested a possible connection between G11.2−0.3 and the "new star" of AD 386. If the association is real, it provides an absolute age for the remnant.

a) Radio Observations of G11.2−0.3

The source G11.2−0.3 was observed with the VLA at 6 and 20 cm with the D- and C-arrays, respectively. This should provide comparable angular resolution at the two frequencies.

[1] The National Radio Astronomy Observatory is operated by Associated Universities, Inc., under contract with the National Science Foundation.

A dissimilarity between the two observations arises from shadowing of one antenna by another, which is more prevalent in the D-array. Data suffering from shadowing were discarded, so that the 6 cm observation has fewer short spacing data points and as a result may be less sensitive to extended structure. This is borne out by the fraction of total flux observed at the two wavelengths: 75% at 6 cm compared to 93% to 20 cm.

The 20 cm image of G11.2 − 0.3 is shown in Figure 1*a*. The most striking feature of the SNR is the nearly circular annulus of emission. The peak-to-peak diameter of the annulus is 3′.5, while the full diameter of the source is 5′. The brightness decreases inside the shell falling to less than 20% of maximum. Near the center of the remnant we see two local maxima of emission. The comparable 6 cm image in Figure 1*b* shows all the same features, confirming the validity of the maps. There is no evidence for spectral changes across the image.

Not surprisingly, we find the emission to be highly polarized at 6 cm. The polarized brightness distribution reveals the same annulus of emission, although there is not a one-to-one correspondence between polarized and total intensity peaks. Interestingly enough, the polarized emission at 6 cm clearly distinguishes between the two central maxima; the eastern maxima is associated with a peak in polarized emission, while little polarized emission originates near the western component. The orientation and magnitude of polarized emission are shown in Figure 2. The data do not suggest a systematic ordering of the magnetic fields.

We have also obtained a neutral hydrogen absorption profile for G11.2 − 0.3 using the VLA. The data were obtained in a 15 minute integration with 13 inner telescopes of the D-configuration. The data were taken in 128 channels, each 12.2 kHz wide. The data are displayed in Figure 3 as the relative flux from the source in each channel. We see strong absorption velocities out to 45 km s^{-1}, and weak absorption is discernible to +55 km s^{-1}. This is consistent with previous data (Radhakrishnan *et al.* 1972). With our improved signal-to-noise ratio, we can also see weak absorption at negative velocities out to −30 km s^{-1}. In effect, we see absorption at all velocities at which significant emission is present. Taken at face value, the data argue for a distance in excess of 26 kpc. Assuming a spin temperature of 100 K, we infer a neutral hydrogen column density of 1×10^{22} cm^{-3}.

b) X-Ray Observations of G11.2–0.3

The source G11.2 − 0.3 was also observed by three instruments on the *Einstein Observatory*; the imaging proportional counter (IPC), the high-resolution imager (HRI) and the monitor proportional counter (MPC). A description of these instruments can be found in Giacconi *et al.* (1979). In brief, the IPC provides images of X-ray from 0.1 to 4 keV, with 1′ angular resolution and limited energy resolution; the HRI provides images of X-rays from 0.1 to 2 keV, with 3″ angular

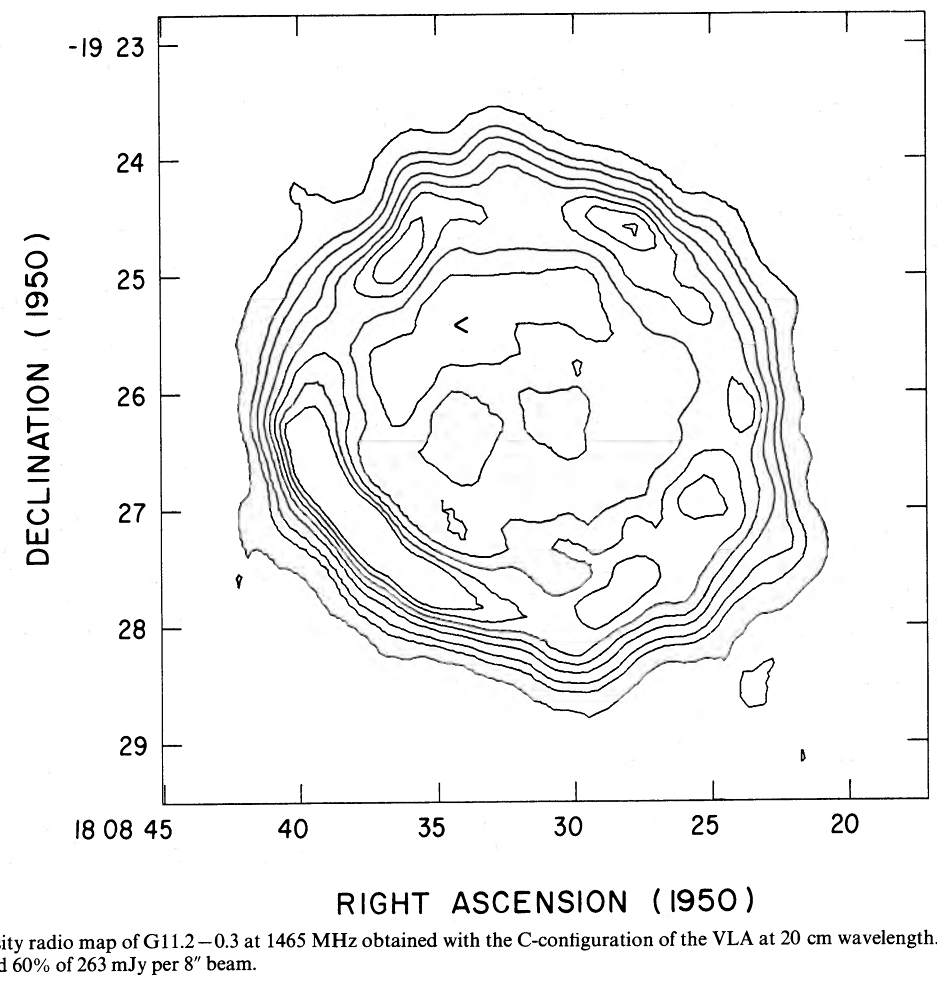

FIG. 1*a*.—Total intensity radio map of G11.2 − 0.3 at 1465 MHz obtained with the C-configuration of the VLA at 20 cm wavelength. Contours are 1%, 5%, 10%, 20%, 30%, 40%, 50%, and 60% of 263 mJy per 8″ beam.

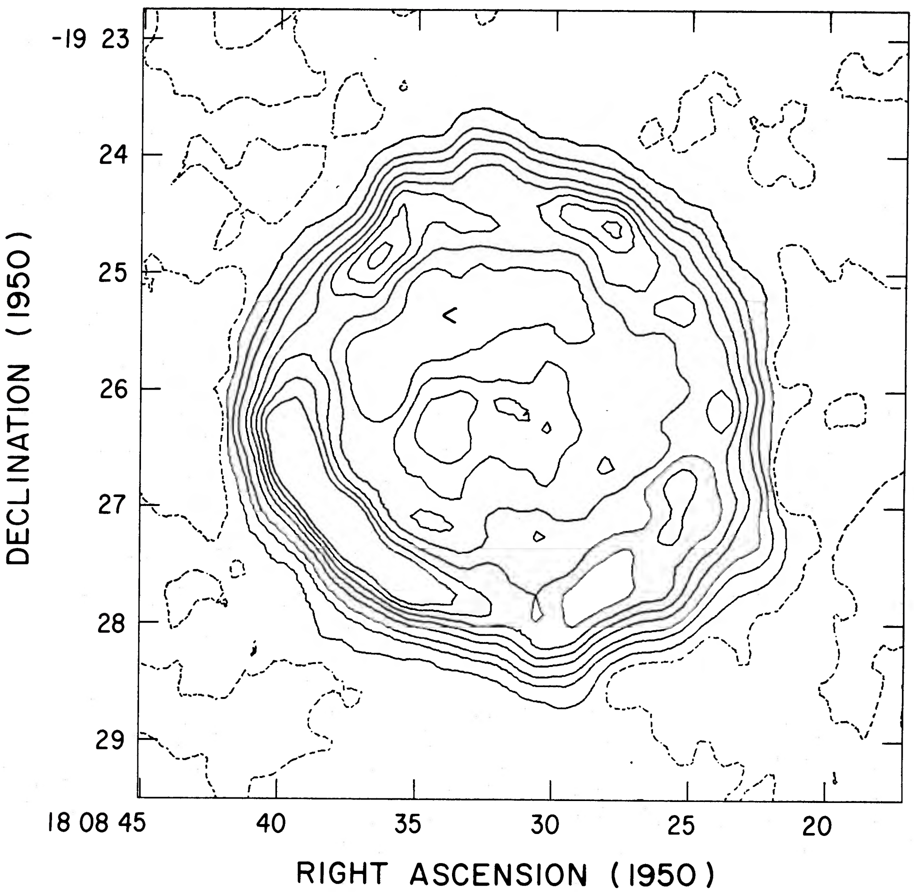

FIG. 1*b*.—Total intensity radio map of G11.2−0.3 at 4885 MHz obtained with the D-configuration of the VLA at 6 cm wavelength. Contours are −1%, 1%, 5%, 10%, 20%, 30%, 40%, 50%, and 60% of 128 mJy per 8″ beam.

resolution and no energy resolution; the MPC provides X-ray spectra from 2 to 15 keV, with no angular resolution save that provided by its beam pattern of 45′.

The IPC observed G11.2−0.3 for 870 s and obtained the image shown in Figure 4. The integrated count rate in the IPC was 0.90 ± 0.03 counts s^{-1}. The image fails to show any shell structure, presumably because of the relatively low angular resolution. The IPC data are consistent with either a thermal or power-law spectrum. The best-fit thermal model (including line emission) between 0.5 and 4.0 keV implies a temperature kT, a column density N_H, and an X-ray intensity of 0.32 keV, 4×10^{22} cm^{-2}, and 2×10^{-11} ergs cm^{-2} s^{-1}, respectively.

Allowing for statistical and gain uncertainties, we find that the IPC data constrain the temperature to lie in the range $0.2 \lesssim kT \lesssim 2.0$ keV and the column density to satisfy $1 \times 10^{22} \lesssim N_H \lesssim 4 \times 10^{22}$ cm^{-2}.

The HRI in a 12,400 s observation also succeeded in detecting the source with an integrated count rate of 0.076 ± 0.005 counts s^{-1}. The HRI image shown in Figure 5 does a much better job of revealing the internal structure of G11.2−0.3. We see clear evidence of the shell with the brightest X-ray component coinciding with the radio peak. In addition, the X-ray map also shows significant central emission near the western of the two central radio components (~10% of the HRI flux is in the central component).

The MPC also detected G11.2−0.3 at a count rate of 2.9 ± 0.2 counts s^{-1} (~2 *Uhuru* flux units in the 2–6 keV range). The MPC data between 1 and 10 keV were best fitted by a thermal model with kT, N_H, and intensity of 3.3 keV, 2.5×10^{21} cm^{-2}, and 5.4×10^{-11} ergs cm^{-2} s^{-1}. The uncertainty ranges for the temperature and column density (~95%) are $2.0 \lesssim kT \lesssim 5.7$ keV and $N_H \lesssim 10^{22}$ cm^{-2}. Although the MPC and IPC data suggests the presence of two spectral components, they are marginally consistent at $kT = 2.0$ keV and $N_H \approx 10^{22}$ cm^{-2}.

III. G41.1−0.3

As in the case of G11.2−0.3, G41.1−0.3 has traditionally been included in SNR catalogs. However, it has suffered from confusion with a galactic H II region which lies ~5′ west of it. Early observations failed to resolve the two unrelated sources leading to a combined spectral index of about −0.25. Once isolated from the nearby H II region, a correct spectral index of −0.5 was found (Clark and Caswell 1976; Green 1974).

Caswell *et al.* (1982) published a 20 cm image of G41.1−0.3 with ~50″ resolution which revealed two areas of emission suggestive of shell structure with an angular diamerer of 3′.6. The distance to G41.1−0.3 has been estimated as greater than 7.5 kpc on the basis of neutral hydrogen absorption measurements (Caswell *et al.* 1975). Applying the Σ–D relation to G41.1 − 0.3, Milne (1979) estimated the distance to be 12.8 kpc. This latter distance implies a linear diameter of 13.4 pc. Caswell *et al.* (1982) point out that only six known shell sources in the galaxy appear to be younger (or brighter or

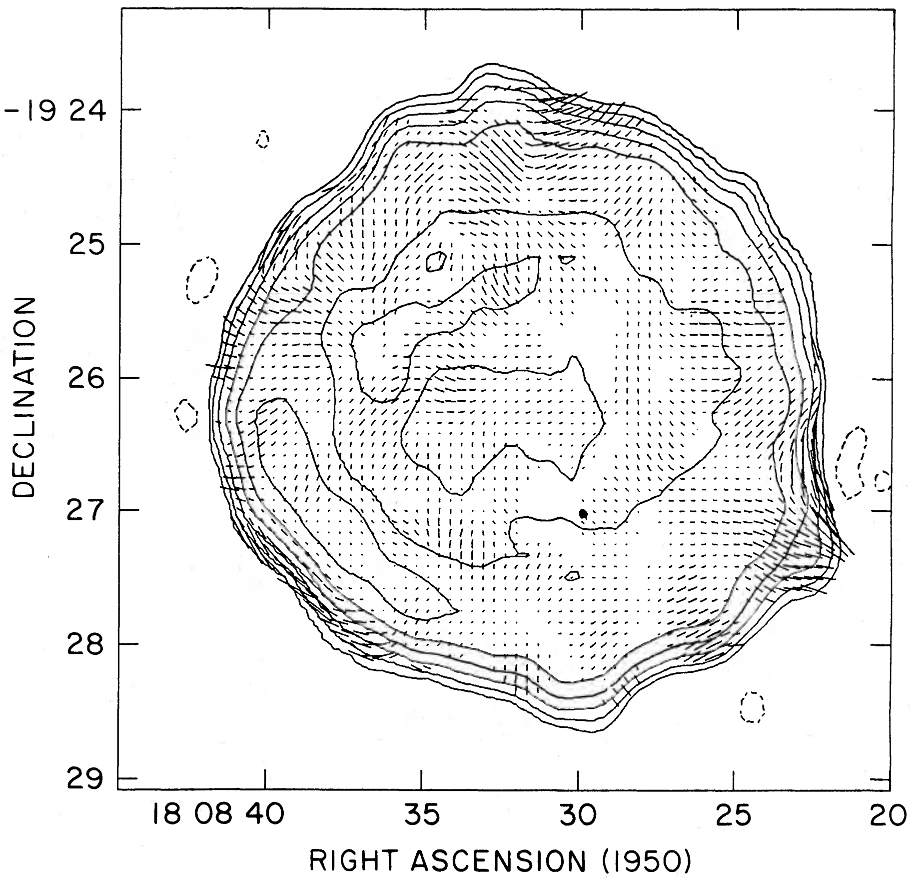

FIG. 2.—Total intensity radio map of G11.2−0.3 at 4885 MHz and 6 cm wavelength with the electric vectors of polarized emission superposed. The length of the vectors indicates the polarized intensity (1″ = 10.5 mJy per beam).

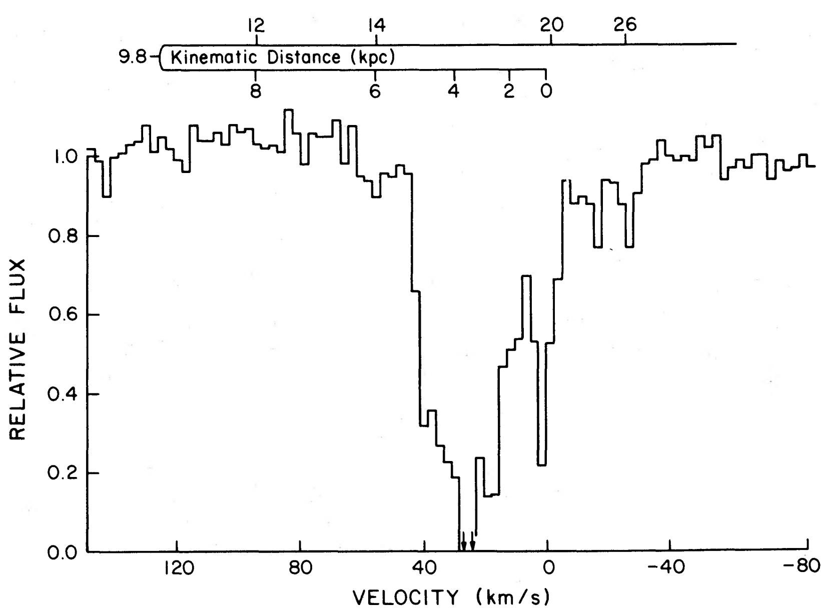

FIG. 3.—Neutral hydrogen absorption profile observed for G11.2−0.3 with the VLA

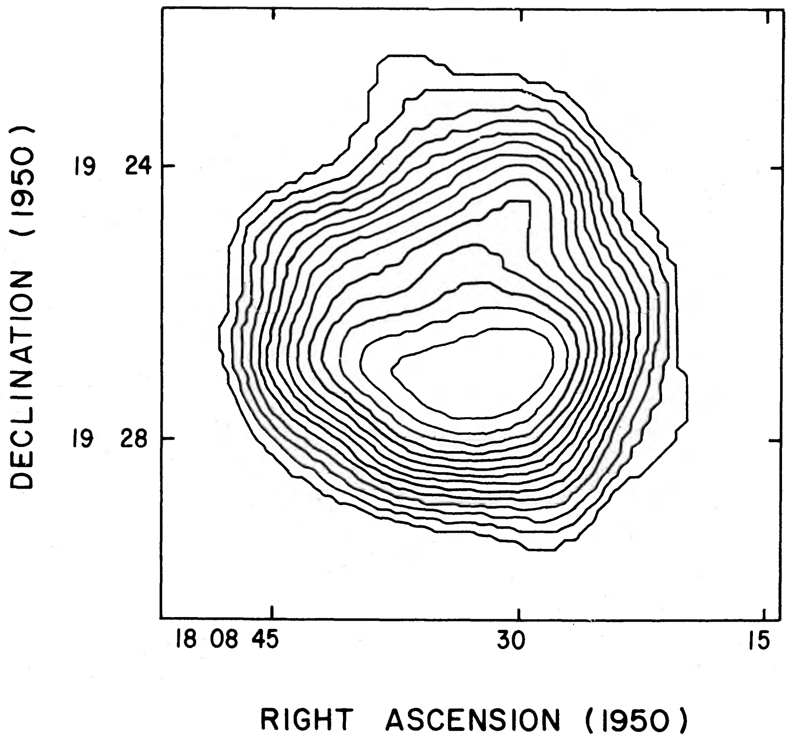

FIG. 4.—Contour map of the X-ray image of G11.2−0.3 obtained with the *Einstein* IPC. Contour levels are 2.8, 4.7, 6.8, 9.1, 11.7, 14.5, 17.5, 20.7, 24.1, 27.8, 31.6, 35.8, 40.1, 44.6, 49.3, and 54.3 counts per 8″ pixel.

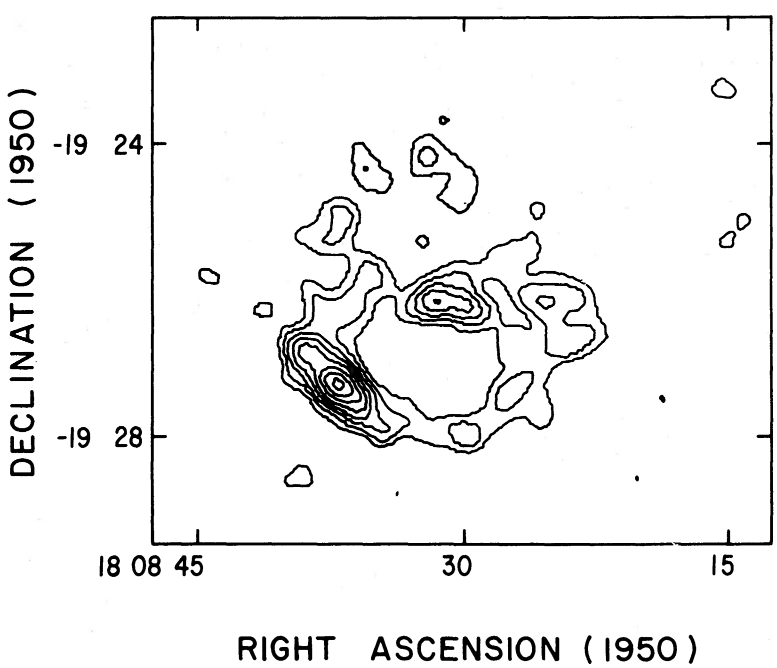

FIG. 5.—Contour map of the X-ray image of G11.2−0.3 obtained with the *Einstein* HRI. Contour levels are 3.7, 5.8, 8.1, 10.4, 12.9, 15.5, 18.3, 21.2, and 24.2 counts per 2″ pixel.

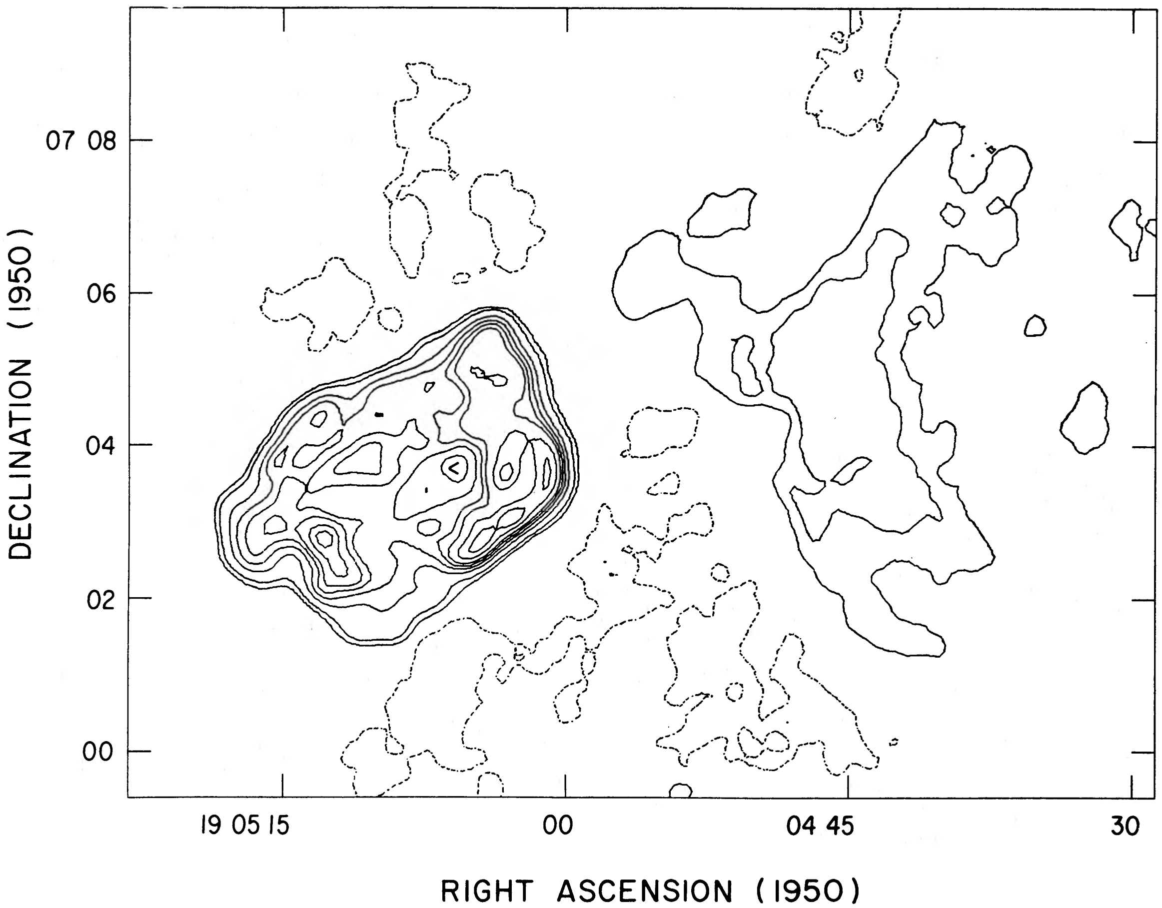

FIG. 6*a*.—Total intensity radio map of G41.1 − 0.3 at 1465 MHz obtained with the C-configuration of the VLA at 20 cm wavelength. Contour levels are −2%, 2%, 5%, 15%, 25%, 35% 45%, 65%, and 85% of 203 mJy per 8″ beam.

smaller) than G41.1 − 0.3, and they suggested an age of under 1000 yr.

a) Radio Observations of G41.1 − 0.3

The observations of G41.1 − 0.3 were made concurrently with those for G11.2 − 0.3 and suffer from the same constraints, although shadowing is less severe at northern declinations. At both 6 and 20 cm we detected 65% of the expected total flux, so the maps should be comparable. The resulting cleaned 6 and 20 cm maps are displayed in Figures 6*a* and 6*b*. The two maps of G41.1 − 0.3 are virtually identical, and we see no evidence for variations in spectral index across the source. The low-level contours to the west are from the adjacent H II region. The remnant has the appearance of a broken shell with a central enhancement and lacks the symmetry one expects of a very young SNR.

We find significant polarization at 6 cm. The peak in polarized intensity occurs interior to the shell coincident with the central enhancement and is equivalent to ∼8% polarization (see display of polarization data in Fig. 6*b*). Secondary peaks in the polarized intensity occur along the western boundary of the remnant.

b) X-Ray Observations of G41.1 − 0.3

The source G41.1 − 0.3 was observed by the IPC, HRI, and MPC. The IPC observation lasted 800 s and recorded an integrated count rate of 0.60 ± 0.03 counts s^{-1}. In comparison, a 3200 s observation by the HRI detected 0.063 ± 0.009 counts s^{-1}. The two resulting images are displayed in Figures 7 and 8. The concurrent MPC observation found 1.44 ± 0.16 counts s^{-1}.

The IPC image shows two concentrations of emission, neither of which appear to correlate with the brightest radio emission region. The HRI image suffers from poor signal to noise and does not appear completely consistent with the IPC results. Both images hint at some emission being associated with the central radio component.

As with G11.2 − 0.3, the IPC spectral fits suggest a spectrum softer than that seen by the MPC, although in this case the two spectral fits do not overlap even at the limits of their uncertainty ranges. The IPC data imply (for a thermal model) $kT < 0.25$ keV and $N_H > 5 \times 10^{22}$ cm^{-2}, while the MPC data are best fitted with kT in the range 1.0 to 6.0 keV and $N_H \leq 1.4 \times 10^{22}$ cm^{-2}. More complex, multicomponent spectral models are clearly appropriate.

IV. DISCUSSION

The results present here reveal the two sources G11.2 − 0.3 and G41.1 − 0.3 as shell supernova remnants. The radio images in both cases reveal some departure from a shell brightness distributions, particularly in the case of G41.1 − 0.3. Neither object shows any indication of a flat-spectrum component

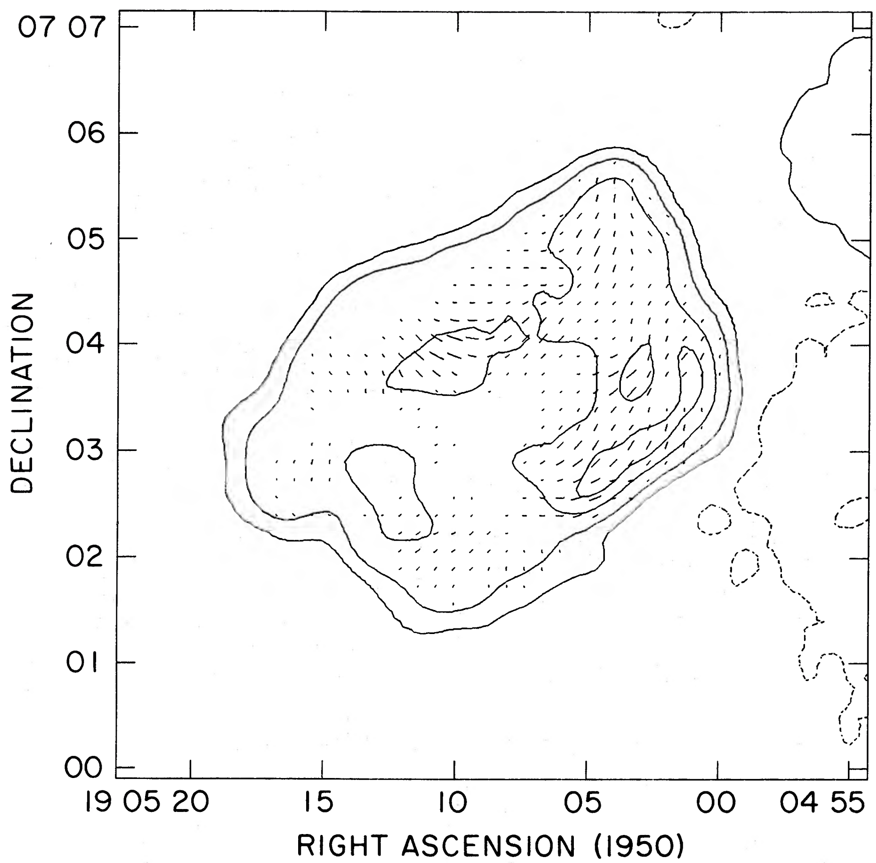

FIG. 6b.—Total intensity radio map of G41.1 − 0.3 obtained at 4885 MHz with the D-configuration of the VLA at 6 cm wavelength. Contour levels are −2%, 2%, 10%, 40%, and 80% of 129 mJy per 8″ beam. Electric vectors of polarized emission are superposed. The length of the vectors indicates the polarized intensity (1″ = 0.6 mJy).

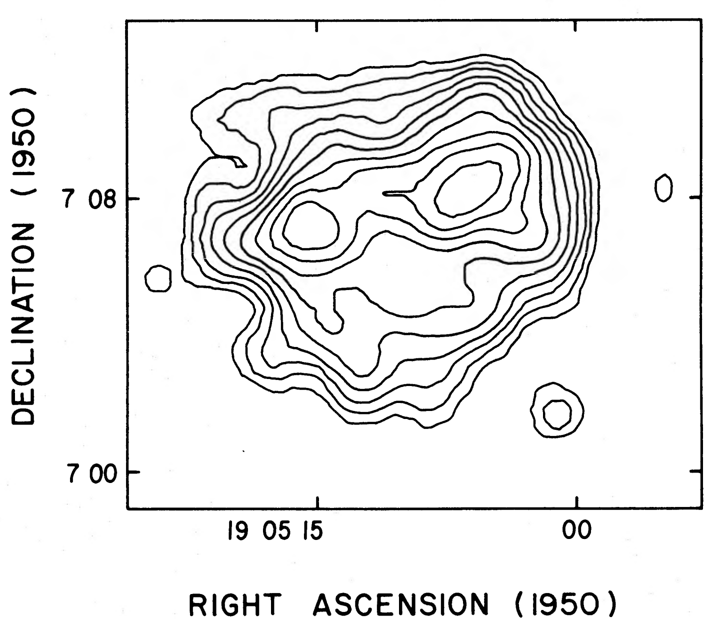

FIG. 7.—Contour map of the X-ray image of G41.1 − 0.3 obtained with the *Einstein* IPC. Contour levels are 4.1, 6.9, 10.5, 14.6, 19.3, 24.5, 30.4, 36.8, 43.8, 51.4, and 59.4 counts per 8″ pixel.

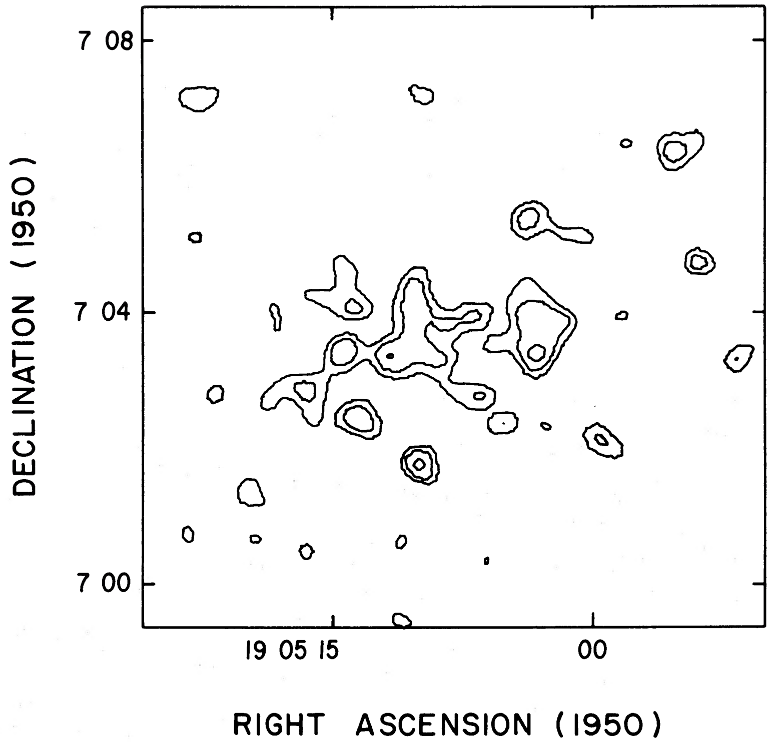

FIG. 8.—Contour map of the X-ray image of G41.1 − 0.3 obtained with the *Einstein* HRI. The contour levels are 1.8, 2.9, 4.2, and 5.5 counts per 2″ pixel.

which might indicate the presence of a central stellar remnant. Certainly the distributions of total and polarized intensities fall within the range of diversity displayed by other well-observed SNRs.

The X-ray data presented here are not of a quality comparable to the radio results. The X-ray brightness distributions are consistent with shell morphologies, but by themselves are not convincing. The spectral data cannot distinguish between thermal and power-law models or, for that matter, provide a good estimate of the neutral hydrogen column density. They do reveal both sources to be relatively bright X-ray sources, implying that future observations could be fruitful.

We would like to acknowledge the assistance of David Helfand and M. Garcia. In addition, R. H. B. acknowledges the support of the National Science Foundation under grant AST-8313685 and the support of NASA under grant NAG8-501, while T. M. and M. D. received support from NASA under grant NAG8-494.

REFERENCES

Andrews, M., Basart, J. P., Lamb, R. C., and Becker, R. H. 1983, *Ap. J.*, **266**, 684.
Becker, R. H., Helfand, D. J., and Szymkowiak, A. E. 1983, *Ap. J.* (*Letters*), **268**, L93.
Becker, R. H., and Szymkowiak, A. E. 1981, *Ap. J* (*Letters*), **248**, L23.
Caswell, J. L., Haynes, R. F., Milen, D. K., and Wellington, J. J. 1982, *M.N.R.A.S.*, **200**, 1143.
Caswell, J. L., Murray, J. D., Roger, R. S., Cole, D. J., and Cooke, D. J. 1975, *Astr. Aps.*, **45**, 239.
Clark, D. H., and Caswell, J. L. 1976, *M.N.R.A.S.*, **174**, 267.
Clark, D. H., and Stephenson, F. R. 1977, *The Historical Supernova* (New York: Pergamon).
Downes, A. 1984, *M.N.R.A.S.*, **210**, 845.
Downes, D. 1971, *A.J.*, **76**, 305.
Giacconi, R., *et al.* 1979, *Ap. J.*, **230**, 540.
Green, A. J. 1974, *Astr. Ap. Suppl.*, **18**, 267.
Helfand, D. J., and Becker, R. H. 1984, *Nature*, **307**, 215.
Ilovaisky, S. A., and Lequeux, J. 1972, *Astr. Ap.*, **18**, 169.
Kriss, J., Becker, R. H., Helfand, D. J., and Canizares, C. 1985, *Ap. J.*, in press.
Milne, D. K. 1979, *Australian J. Phys.*, **32**, 83.
Pye, J. P., Becker, R. H., Seward, F. D., and Thomas, N. 1984, *M.N.R.A.S.*, **207**, 649.
Radhakrishnan, V., Goss, W. M., Murray, J. D., and Brooks, J. W. 1972, *Ap. J. Suppl.*, **24**, 49.
Shaver, P. A., and Weiler, K. K. 1976, *Astr. Ap.*, **53**, 237.

R. H. BECKER: Physics Department, University of California, Davis, CA 95616

M. DONAHUE and T. MARKERT: Center for Space Research, MIT, Cambridge, MA 02139